A Conformational Change in F-Actin When Myosin Binds: Fluorescence Resonance Energy Transfer Detects an Increase in the Radial Coordinate of Cys-374[†]

Pierre D. J. Moens* and Cristobal G. dos Remedios

Muscle Research Unit, Department of Anatomy and Histology, Institute for Biomedical Research, The University of Sydney, Sydney 2006, Australia

Received October 15, 1996; Revised Manuscript Received April 3, 1997[⊗]

ABSTRACT: Interactions of myosin with actin filaments probably induce conformational changes in actin which are crucial for its function. Fluorescence resonance energy transfer spectroscopy can determine changes in distance (range 10−100 Å) between two probes and therefore can sense conformational changes in proteins. We have investigated changes in the radial coordinates of fluorescent probes bound to Cys-374 of F-actin when either of the isozymes (S1A1 and S1A2) of myosin subfragment 1 (S-1) bind. Using 5-[[2-[(iodoacetyl)amino]ethyl]amino]naphthalene-1-sulfonic acid and *N*-(4-dimethylamino-3,5-dinitrophenyl)maleimide as donor and acceptor probes, respectively, we calculated a radius of 13−14 Å. This distance increased by ≈4.5 Å upon addition of S-1. No differences were detected between the effects of S1A1 and S1A2. This increase is reversed by MgATP. The average position of the probes on Cys-374 is closer to the filament axis than expected from the current models of F-actin. S-1 increases the radial position of Cys-374 either by direct interaction or via an allosteric conformational change associated with its binding.

In muscles, myosin interacts with actin filaments (F-actin)[1] to produce contractile force. Recently, the atomic structures of both monomeric actin (Kabsch et al., 1990) and subfragment 1 of myosin (S-1) (Rayment et al., 1993) have been published. The structure of rabbit skeletal muscle actin was solved at 2.8 Å resolution by Kabsch et al. (1990) using crystals of actin complexed with DNase I. To facilitate the crystallization, the C-terminal three residues (including Cys-374) were removed using mild tryptic digestion (Mannherz et al., 1977). In 1993, two other actin structures were published; one when undigested actin was complexed with gelsolin segment 1 (McLaughlin et al., 1993) and the other with profilin (Schutt et al., 1993). These structures are almost identical to that determined by Kabsch, and they leave little doubt about the consensus structure [for a review, see dos Remedios and Moens (1995a)].

F-Actin does not readily form crystals. Consequently, its structure must be determined using other methods. Monomeric actin structure has been used to build models of F-actin (Holmes et al., 1990; Lorenz et al., 1993; Tirion et al., 1995). Holmes et al. (1990) completed the Kabsch atomic structure by reconstructing the last three residues of the C-terminus, and the atomic map of the monomeric actin was fitted onto X-ray diffraction data of flow-oriented gels of phalloidin-stabilized F-actin. This model locates the large domain (comprising subdomains 3 and 4) at a low radius from the filament axis and places the small domain (subdomains 1 and 2) closer to the periphery of the filament. The model emphasizes the contact between monomers along the two-start, long-pitch helices. Other models differ only subtly from the 1990 Holmes model with alterations in the DNase I-binding loop, the hydrophobic loop (residues 264−273), and/or in the region near residues 81−90 (Lorenz et al., 1993; Mendelson & Morris, 1994; Tirion et al., 1995).

Actin filaments are flexible, and binding of S-1 increases their flexibility (Yanagida & Oosawa, 1978). This change is probably essential for its function because chemical cross-linking of F-actin with glutaraldehyde inhibits the sliding of filaments in a motility assay (Prochniewicz-Nakayama & Yanagida, 1990).

S-1 binding is known to modify actin structure. When actin is decorated with S-1, the radial coordinate of Gln-41 in subdomain 2 of actin increases by 4−5 Å (Kasprzak et al., 1988). In a separate report, the distance between the nucleotide locus and Tyr-69 in subdomain 2 also increases by approximately 4 Å (Miki & Kouyama, 1994). In three-dimensional reconstructions from electron micrographs of actin filaments, Orlova and Egelman (1995) detected a bridge of density which they believed arises from a major shift of the C-terminus. This bridge is present in Ca^{2+}−F-actin but absent in Mg^{2+}−F-actin. They also proposed that the conformational change when this bridge forms may be induced by myosin binding. In the G-actin−DNase I crystal structure, the truncated C-terminus is highly mobile (Kabsch et al., 1990). We recently determined the average position of a fluorescent probe attached to Cys-374 to be at a radius of 17−18 Å from the long axis of the filament (Moens et al., 1994). This is somewhat smaller than the 26 Å predicted by the Lorenz filament model (Lorenz et al., 1993).

[†] This research was funded by a grant from the National Health & Medical Research Council of Australia.

* Corresponding author. E-mail: pierre@anatomy.su.oz.au. Phone: 61-2-93516543. Fax: 61-2-93512813.

[⊗] Abstract published in *Advance ACS Abstracts,* May 15, 1997.

[1] Abbreviations: F-actin, actin filament; S-1, myosin subfragment 1; G-actin, globular actin; A1, A2, essential light chains 1 or 2; S1A1, S1A2, S-1 isomers carrying light chains A1 or A2; FRET, fluorescence resonance energy transfer; 1,5-IAEDANS, 5-[[2-[(iodoacetyl)amino]-ethyl]amino]naphthalene-1-sulfonic acid; DDPM, *N*-(4-dimethylamino-3,5-dinitrophenyl)maleimide; DABMI, 4-[[[4-(dimethylamino)phenyl]-azo]phenyl]maleimide; AMF, acceptor molar fraction.

S0006-2960(96)02588-3 CCC: $14.00

Table 1: Examples of the Determination of Acceptor Molar Fractions[a]

	A-labeled actin vol (mL)	D-labeled actin vol (mL)	concn of DABMI-labeled actin (μM)	concn of DDPM-labeled actin (μM)	concn of IAEDANS-labeled actin (μM)	D probe concn (μM)	A probe concn (μM)	total actin concn (μM)	AMF A concn/-tot concn (mM)
1	0.9	0.1	42.2	−	4.9	4.3	24.4	47.1	0.52
2	0.7	0.3	32.8	−	14.8	12.8	19.0	47.6	0.40
3	0.5	0.5	23.4	−	24.7	21.4	13.6	48.1	0.28
4	0.9	0.1	−	48.5	4.9	4.3	28.7	53.4	0.54
5	0.7	0.3	−	37.7	14.8	12.8	22.3	52.5	0.42
6	0.5	0.5	−	26.9	24.7	21.4	15.9	51.6	0.31

[a] The final volume for each sample was 1 mL. The labeling ratios for DABMI, DDPM, and IAEDANS labeled actin were 0.58, 0.60, and 0.87, respectively. The protein and probe concentrations were obtained as described under Materials and Methods. A, acceptor; D, donor; vol, volume; concn, concentration; tot, total actin.

S-1 exists in two isoforms, S1A1 and S1A2, depending on its associated essential light chain. Myosin light chain 1 (LC1) in S1A1 has a 41 amino acid sequence extension [compared to myosin light chain 3 (LC3) in S1A2] which allows it to associate with actin. Using proton NMR, Trayer et al. (1987) showed that the N-terminal region of myosin light chain 1 interacts directly with the actin C-terminus. However, recently, Xiao et al. (1996) found that S1A1 and S1A2 had a different polarization when bound to unsaturated filaments but had the same polarization when bound to saturated filaments. They concluded that in S-1-saturated F-actin neither LC1 nor LC3 light chain interacts with actin.

Fluorescence resonance energy transfer (FRET) spectroscopy has been used to measure radial coordinates of probes bound to F-actin (Kasprzak et al., 1988; Miki & dos Remedios, 1990; Miki et al., 1986; Moens et al., 1994; Taylor et al., 1981). The precision of these measurements is impaired by several factors: the unknown nature of the orientation factor, nonrandom polymerization of the labeled monomers, and the relatively large size of some probes. The orientation factor problem has been discussed elsewhere and can be assumed to be equal to $^2/_3$ (Censullo et al., 1992; dos Remedios & Moens, 1995b). In the worst case, the intramolecular distance error in F-actin will be less than 20% (Censullo et al., 1992). Labeling of actin monomers can result in nonrandom polymerization, but this can be avoided by judicious selection of the probes and by the inclusion of phalloidin during polymerization (Moens et al., 1994). Most of the probes used in FRET are sizable (with a maximum cord of up to 15 Å) compared to the proteins to which they are attached. Thus, probe size has to be taken into account when interpreting the results. However, FRET makes up for this deficit by being very good at detecting structural changes in proteins (dos Remedios & Moens, 1995b) and can resolve changes of about 1 Å in probe position. In this work, we show that the average radial coordinate of probes covalently bound to Cys-374 in F-actin increases when either myosin S1A1 or S1A2 saturates actin filaments.

MATERIALS AND METHODS

Preparation of Actin and Myosin. Actin was prepared from an acetone powder of rabbit skeletal muscle by the method of Spudich and Watt (1971) with minor modifications (Barden & dos Remedios, 1984). Myosin was prepared using the method described by Tonomura et al. (1966), and the myosin S-1 isoforms (S1A1 and S1A2) were prepared and separated according to Weeds and Taylor (1975). The concentrations of unlabeled G-actin and S-1 isoforms were determined spectrophotometrically using extinction coefficients of $\epsilon = 6.3$ cm^{-1} (0.1%, 290 nm) and $\epsilon = 7.5$ cm^{-1} (0.1%, 280 nm), respectively.

Labeling of Actin. Cys-374 was labeled with 1,5-IAEDANS as described in dos Remedios and Cooke (1984). The labeling of Cys-374 with the acceptor probes DDPM or DABMI was according to the methods of Miki and Mihashi (1978) and Barden and dos Remedios (1987), respectively. To remove the unbound labels, actin was put through a polymerization−depolymerization cycle, dialyzed in the presence of 1% dimethylformamide, clarified at 130000*g* for 60 min at 4 °C, and then passed through a G-25 Sephadex column (2 × 10 cm). The concentration of the labeled actin was determined from the absorbance at 595 nm using the Coomassie protein assay reagent (Bradford, 1976). A range of actin concentrations was used to construct a standard curve. The following extinction coefficients for the labeled proteins were used (M^{-1} cm^{-1}): 1,5-IAEDANS, $\epsilon_{336} = 6.1 \times 10^3$ (Hudson & Weber, 1973); DDPM, $\epsilon_{440} = 3.0 \times 10^3$ (Miki & Mihashi, 1978); DABMI, $\epsilon_{460} = 2.48 \times 10^4$ (dos Remedios et al., 1987). Labeling efficiencies ranged from 0.5 to 1. 1,5-IAEDANS and DABMI were purchased from Molecular Probes Inc., and DDPM was from Aldrich Chemical Co. The determination of Cys-374 as the uniquely labeled cysteinyl has been described in Moens et al. (1994).

Determination of the Acceptor Molar Fraction. Donor- and acceptor-labeled actins were mixed to obtain multiple acceptor molar fractions (AMF). This was achieved by mixing increasing amounts of acceptor-labeled actin with decreasing amounts of donor-labeled actin such that the volume of each sample was 1 mL. Then, the AMF were calculated from the concentration of acceptor and total actin in each sample. Examples of the determination of the AMF are shown in Table 1.

Polymerization of Actin. Following the fluorescence measurements of the unpolymerized actin solutions, phalloidin was added in a 2 molar excess over actin and polymerized by the addition of 20 mM phosphate buffer, pH 7.0, 50 mM KCl, and 2 mM $MgCl_2$. After 1.5−2 h at room temperature, the fluorescence of the polymerized actin solution was recorded. After sedimentation experiments, less than 1 μM of probes were detected in the supernatant, and the actin concentrations were beyond the detection level of the Bradford assay (data not shown). Myosin was added to obtain a 1.5 molar excess over actin. Myosin was mixed with actin solution and was allowed to stand for 30 min prior to fluorescence measurements. In some samples, the fluorescence was recorded following the addition of 10 mM ATP.

Fluorescence Measurements. We used both lifetime and steady-state measurements. The lifetimes of the donor probe

Table 2: Calculation of Transfer Efficiency in an Actin Filament[a]

	acceptor environment (n)						
k	−2	−1	0	1	2	probability, δ_k	efficiency of transfer, E_k
1	−	−	D	−	−	$(1-p)^4$	0
2	A	−	D	−	−	$p(1-p)^3$	$R_0^6\{R_0^6+R_{-2}^6\}^{-1}$
3	−	A	D	−	−	$p(1-p)^3$	$R_0^6\{R_0^6+R_{-1}^6\}^{-1}$
4	−	−	D	A	−	$p(1-p)^3$	$R_0^6\{R_0^6+R_1^6\}^{-1}$
5	−	−	D	−	A	$p(1-p)^3$	$R_0^6\{R_0^6+R_2^6\}^{-1}$
6	A	A	D	−	−	$p^2(1-p)^2$	$R_0^6\{R_0^6+1/[R_{-2}^{-6}+R_{-1}^{-6}]\}^{-1}$
7	A	−	D	A	−	$p^2(1-p)^2$	$R_0^6\{R_0^6+1/[R_{-2}^{-6}+R_1^{-6}]\}^{-1}$
8	A	−	D	−	A	$p^2(1-p)^2$	$R_0^6\{R_0^6+1/[R_{-2}^{-6}+R_2^{-6}]\}^{-1}$
9	−	A	D	A	−	$p^2(1-p)^2$	$R_0^6\{R_0^6+1/[R_{-1}^{-6}+R_1^{-6}]\}^{-1}$
10	−	A	D	−	A	$p^2(1-p)^2$	$R_0^6\{R_0^6+1/[R_{-1}^{-6}+R_2^{-6}]\}^{-1}$
11	−	−	D	A	A	$p^2(1-p)^2$	$R_0^6\{R_0^6+1/[R_1^{-6}+R_2^{-6}]\}^{-1}$
12	A	A	D	A	−	$p^3(1-p)$	$R_0^6\{R_0^6+1/[R_{-2}^{-6}+R_{-1}^{-6}+R_1^{-6}]\}^{-1}$
13	A	A	D	−	A	$p^3(1-p)$	$R_0^6\{R_0^6+1/[R_{-2}^{-6}+R_{-1}^{-6}+R_2^{-6}]\}^{-1}$
14	A	−	D	A	A	$p^3(1-p)$	$R_0^6\{R_0^6+1[R_{-2}^{-6}+R_1^{-6}+R_2^{-6}]\}^{-1}$
15	−	A	D	A	A	$p^3(1-p)$	$R_0^6\{R_0^6+1/[R_{-1}^{-6}+R_1^{-6}+R_2^{-6}]\}^{-1}$
16	A	A	D	A	A	p^4	$R_0^6\{R_0^6+1/[R_{-2}^{-6}+R_{-1}^{-6}+R_1^{-6}+R_2^{-6}]\}^{-1}$

[a] From O'Donoghue et al. (1991). A donor attached at the $n = 0$ monomer can transfer to an acceptor group at the *n*th FRET locus on the four nearest monomers ($n = -2, -1, 1, 2$). Each of these monomers may (A) or may not (−) be labeled with acceptors; thus, there are 16 different possible acceptor environments. The probability for each arrangement, δ_k, is given as a function of *p*, the acceptor molar fraction. The transfer efficiency for each arrangement, E_k, is a function of the intermonomer distances R_{-2}, R_{-1}, R_1, and R_2 (see eq 3).

were recorded using a photon counting EEY nanosecond fluorometer. The excitation wavelength was selected using a band-pass filter centered at 350 nm with a band-pass of 80 nm, and the emission wavelength was selected using a filter which transmits above 410 nm.

The steady-state measurements were recorded using an SLM-8000 photon-counting spectrofluorometer operated in the ratio mode. 1,5-IAEDANS was excited at 336 nm, and the emission spectra were recorded at 400−600 nm. Samples were temperature-controlled at 16 °C.

Theoretical Calculations. The radial coordinate of the probe bound to Cys-374 was determined using the method described by Taylor et al. (1981). The FRET efficiency (*E*) depends on the distance (*R*) separating the dipole moments of the donor and acceptor probes according to the equation:

$$E = \frac{R_0^6}{R_0^6 + R^6} \tag{1}$$

where R_0 is the Förster critical distance (the distance at which the efficiency of energy transfer is 50%). For the 1,5-IAEDANS−DDPM probe pair, we used the R_0 value of 29 Å published by Dalbey et al. (1984) and the value of 42.8 Å calculated by Kasprzak for the 1,5-IAEDANS−DABMI probe pair (Kasprzak et al., 1988).

FRET efficiency in an actin filament is given by

$$E_f = \sum_{k=1}^{K} \delta_k E_k \tag{2}$$

where *K* is the number of possible arrangements of acceptor-labeled monomers around a donor-labeled monomer and in our case is equal to 16 because of the known symmetry of the actin filament (Moens et al., 1994). δ_k is the probability of the *k*th arrangement, and E_k is the efficiency of transfer for that arrangement. The probability and efficiency of transfer for each arrangement are given in Table 2.

The distance (*R*) between a donor probe ($n = 0$) and an adjacent acceptor probe ($n = -2, -1, 1$, or 2) for a given radius (*r*) is given by

$$R_n = [r^2(1 - \cos(n*166°))^2 + r^2 \sin^2(n*166°) + (n*27.5)^2]^{1/2} \tag{3}$$

From eqs 1 and 3, we can calculate theoretical FRET efficiencies against AMF over a range of radii (*r*).

Data Analysis. From Table 2, one can see that the transfer efficiency will vary for each arrangement of acceptor around a donor. However, due to the helical symmetry of the actin filament, some acceptor environments will give the same transfer efficiency; e.g., the efficiency of transfer between a donor and an acceptor located on monomer $n-2$ will be the same as the transfer efficiency between a donor and an acceptor on monomer $n+2$. Therefore, the 16 different possible arrangements will reduce to 9 different efficiencies of transfer and hence 9 different donor lifetimes. The observed lifetime for a filament will then be a sum of 9 lifetimes where their proportions are a function of the AMF.

The theoretical calculation of the efficiency of transfer for a given radius as a function of the AMF is obtained by measuring the observed FRET efficiency of the solution. This is valid when measuring the steady-state fluorescence intensity, but what happens with the lifetime analysis? We have computed theoretical lifetimes for various AMF for four different radii using a donor-alone lifetime of 20 ns and analyzed them with either one- or two-exponential decay curves. The FRET efficiency for the two-exponential analysis is calculated using the shortest of the two lifetimes. The results are shown in Figure 1: the open triangles are the FRET efficiencies obtained assuming a single lifetime,

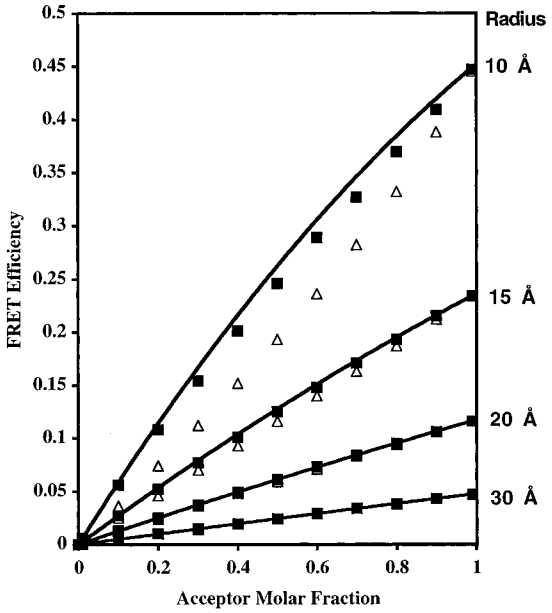

FIGURE 1: Computed efficiencies of transfer in an actin filament for radii ranging from 10 to 30 Å. The lifetime data were calculated using a donor probe lifetime of 20 ns, and the theoretical curves for the different radii were obtained for the multiple AMF with an R_0 value of 29 Å. (■) are the values obtained from the analysis of the lifetimes assuming a double-exponential decay curve, and the FRET efficiencies were calculated using the shortest of the two lifetimes. (△) are the results obtained when the data were analyzed assuming a single-exponential decay.

and the filled squares are obtained assuming two lifetimes. For a small efficiency of transfer, the two methods give the same results (Figure 1, curves 20 and 30 Å) while for a higher efficiency of transfer (curves 15 and 10 Å) the fit is much better when we assume two lifetimes. However, for high efficiencies of transfer, this method of analysis will result in a small overestimation of the radial coordinates of the probes. At low AMF, the longer of the two lifetimes approaches the value of the lifetime of the unperturbed donor (data not shown). However, as the lifetime curves are a sum of nine exponentials, the components obtained with a two-exponential analysis have no physical significance.

Modifications of the fluorescence lifetimes and intensities of the samples were corrected for the effects of the polymerization of actin and/or the addition of S-1, or MgATP, using solutions containing donor-labeled actin only. No differences in the lifetimes of the "donor only" solutions could be detected between the different concentrations of donor in the solutions (data not shown); therefore, donor to donor transfer can be disregarded. These donor to donor transfers are also called homotransfer and cannot be detected from the quenching of the donor fluorescence, from the spectra, and from the time dependence of the intensity (lifetime) because of the symmetry of the situation: If one molecule gives its excitation energy to another of the same species, the second will have the same fluorescence characteristic as the first and will merely reemit the energy or pass it on (or back), so that after a few transfers emission will occur as if no transfer had taken place (Van Der Meer et al., 1994). However, if these processes fail to be detected, they nevertheless occur, and each homotransfer contributes to the broadening of the angular distribution of emission dipoles (Van Der Meer et al., 1994) which is in favor of the assumption that κ^2 equals $^2/_3$ in actin filaments.

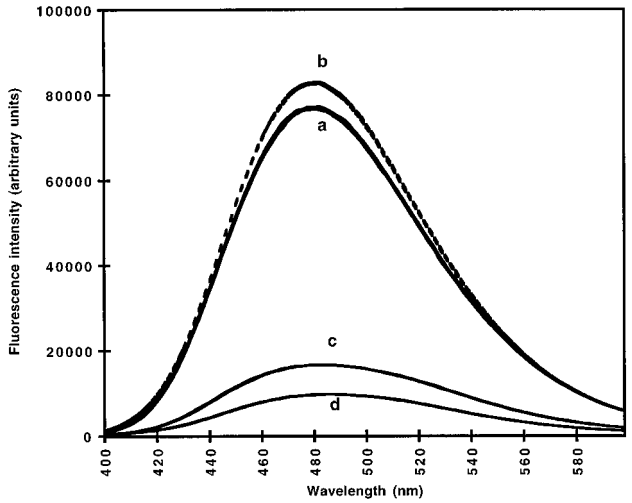

FIGURE 2: Fluorescence spectrum of 1,5-IAEDANS in the presence and absence of DABMI. Each curve is the superimposition of three measurements. Curve a is the emission spectrum from 400 to 600 nm of 1,5-IAEDANS in G-actin without acceptor (donor labels concentration = 43 μM). Cuve b represents the fluorescence intensity of 1,5-IAEDANS without acceptor after polymerization. The emission scan of 1,5-IAEDANS in the presence of DABMI at an acceptor molar fraction of 0.4 (donor labels concentration = 12.8 μM) in G-actin is shown by curve c and in F-actin by curve d.

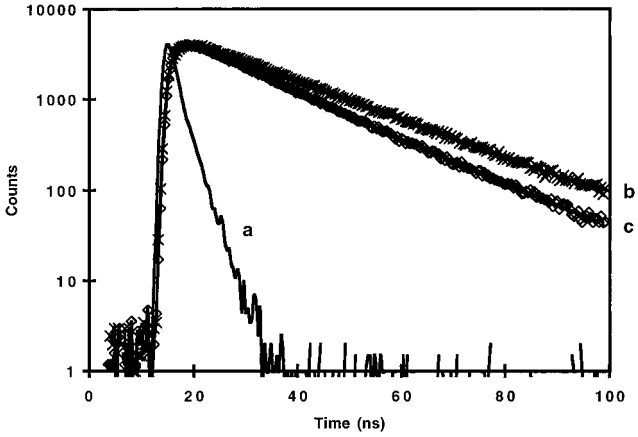

FIGURE 3: Fluoresence lifetime data of 1,5-IAEDANS in the absence and presence of DDPM in F-actin. Trace a is the lamp signal obtained using a scattering solution. (×) symbols are the lifetime data of 1,5-IAEDANS without acceptor. A single-exponential decay curve has been fitted through these points with a lifetime of 20.1 ns (solid line b). (◇) symbols represent the lifetime data from 1,5-IAEDANS in the presence of DDPM at an acceptor molar fraction of 0.55. Two-exponential decay curves have been fitted (solid line c) with the following lifetime parameters: $\alpha_1 = 0.4$, $\tau_1 = 16.4$ ns; and $\alpha_2 = 0.6$, $\tau_2 = 17.6$ ns.

RESULTS

Changes in Fluorescence Due to Polymerization. The fluorescence spectra from the steady-state measurements of 1,5-IAEDANS-labeled G-actin without an acceptor are illustrated by curve a in Figure 2. Upon polymerization, the fluorescence intensity increases by 7% (curve b), which could result from a small change in the environment of the probe, as Cys-374 is close to an actin−actin binding site. The emission peaks of both curves occur at 480−482 nm. The lifetime data of actin labeled with donor only are represented by trace b in Figure 3. As shown in Table 3, the lifetime of 20.1 ns obtained for the F-actin sample containing only donor (acceptor molar fraction: AMF = 0.0) is not significantly

Table 3: Lifetimes (ns) of 1,5-IAEDANS-Labeled Actin with Different Concentrations of DDPM Label[a]

AMF	G-actin	F-actin	+S1A1	+S1A2	+MgATP
0.0	20.0	20.1	20.7	20.7	−
0.18	20.0	18.6	19.6	19.9	−
0.31	20.0	18.1	19.3	19.4	−
0.43	19.9	17.1	18.7	18.7	−
0.55	19.9	16.4	18.1	18.2	14.3

[a] AMF: acceptor molar fraction (concentration of acceptor-labeled monomer versus actin concentration). +S1A1 indicates the presence of myosin subfragment 1 containing myosin light chain 1; +S1A2 is similar except it contains myosin light chain 3.

Table 4: Transfer Efficiencies and Their Corresponding Radii for 1,5-IAEDANS−DABMI and 1,5-IAEDANS−DDPM Probe Pairs Using Steady-State Measurements[a]

acceptor		F-actin		+S-1		+MgATP	
probe	AMF	*E*	radius (Å)	*E*	radius (Å)	*E*	radius (Å)
DABMI	0.40	0.46	15	0.23	24	0.29	21
DDPM	0.42	0.17	12	0.08	17	0.19	11.3

[a] AMF, acceptor molar fraction; *E*, efficiency of transfer. +S-1 indicates the presence of myosin subfragment 1.

different from those of G-actin (19.9−20.0 ns). A lifetime of 20 ns agrees well with the lifetime of 1,5-IAEDANS (21.6 ns) determined in F-actin (Kasprzak et al., 1988). These data suggest there is no dramatic change in the environment of the 1,5-IAEDANS probe fixed to Cys-374 when actin polymerizes.

Radial Coordinate of Cys-374. Increasing concentrations of acceptor in the actin solutions do not modify the lifetime of the donor probe (Table 3). Indeed, with G-actin there is no significant chance of an acceptor probe on one monomer being within 100 Å of a donor probe on another monomer, and thus FRET efficiency will be zero. However, when actin is polymerized, the lifetime of the donor decreased in proportion to the increase in AMF. The data obtained from the 1,5-IAEDANS−DDPM probe pair with an AMF of 0.55 are shown in Figure 3 (diamonds) and have been fitted with two exponentials: $\alpha_1 = 0.4$, $\tau_1 = 16.4$ ns; $\alpha_2 = 0.6$, $\tau_2 = 17.7$ ns (curve c). The calculated transfer efficiency is 0.177, which corresponds to a radial coordinate for the probe pair of 13.5 Å. Similar results were obtained with the steady-state measurements. The fluorescence intensity spectrum of the 1,5-IAEDANS−DABMI probe pair with an AMF of 0.4 is shown in Figure 2. Curve c is the spectrum for G-actin, and curve d is the spectrum following polymerization. The G-actin curve c has a lower peak value of fluorescence intensity than expected from the ratios of the donor concentrations when compared with the donor-only curve a. This difference could result from an inner filter effect of the DABMI probes. Such an effect is not seen in the DDPM samples (data not shown). The inner filter effect can be ignored when comparing G- and F-actin fluorescence intensities because they both have the same acceptor concentration. However, a correction for the inner filter effect is needed when comparing the results obtained for F-actin with and without S-1, as the acceptor concentrations are different due to the addition of S-1. After correction for the increase of fluorescence due to polymerization, we calculated a transfer efficiency of 0.46, corresponding to a radial coordinate of 15 Å (Table 4). We obtained a smaller radius (12 Å) using DDPM as the acceptor probe. The

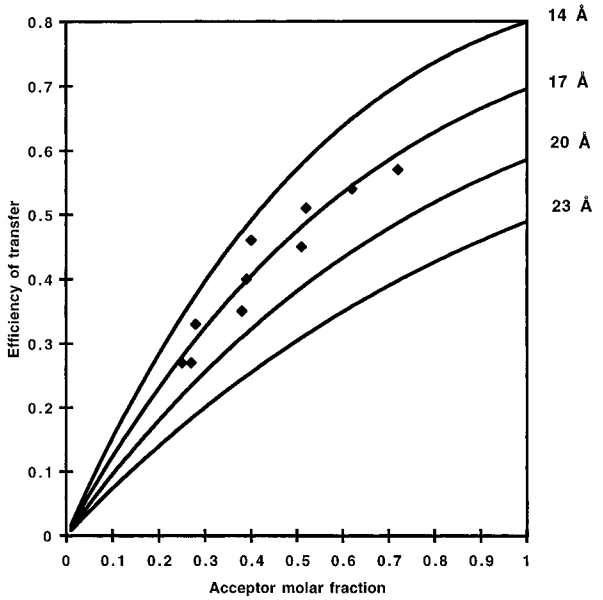

FIGURE 4: Transfer efficiencies observed for various acceptor molar fractions using the 1,5-IAEDANS−DABMI probe pair. The theoretical curves calculated for some radii between 14 and 23 Å are plotted (solid lines). (◆) represent the FRET data for various acceptor molar fractions.

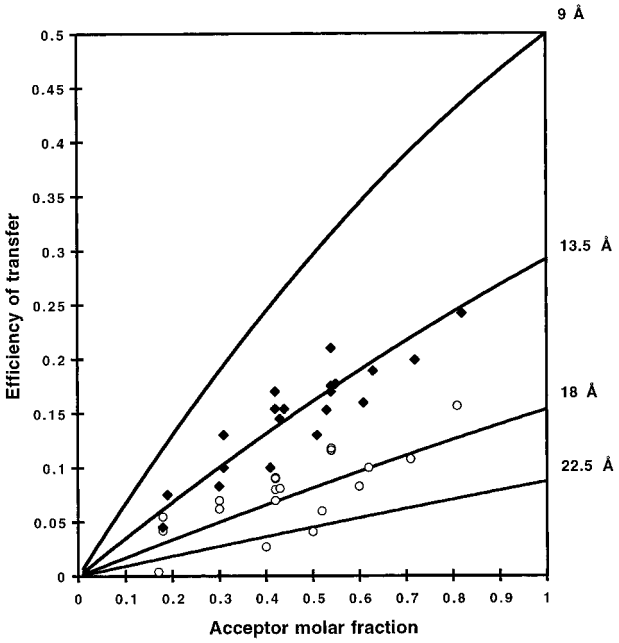

FIGURE 5: Transfer efficiencies observed for various acceptor molar fractions using the 1,5-IAEDANS−DDPM probe pair. The theoretical curves calculated for radii between 9 and 22.5 Å are plotted (solid lines). (◆) symbols represent the FRET data for various acceptor molar fractions in F-actin. (○) symbols are the FRET data in the presence of S-1.

calculated FRET efficiencies from steady-state and lifetime measurements were pooled. The data are plotted with the theoretical curves as shown in Figure 4 for the 1,5-IAEDANS−DABMI probe pair and in Figure 5 for the 1,5-IAEDANS−DDPM probe pair. FRET data obtained with DABMI as the acceptor gave a radial coordinate of 17 ± 2 Å (Figure 4) which agrees with our previous measurements (Moens et al., 1994).

As shown in Figure 5 (◆), a smaller radial coordinate of 13.5 ± 2 Å is obtained for the dipole moment of the 1,5-IAEDANS−DDPM probes. This difference in radius is

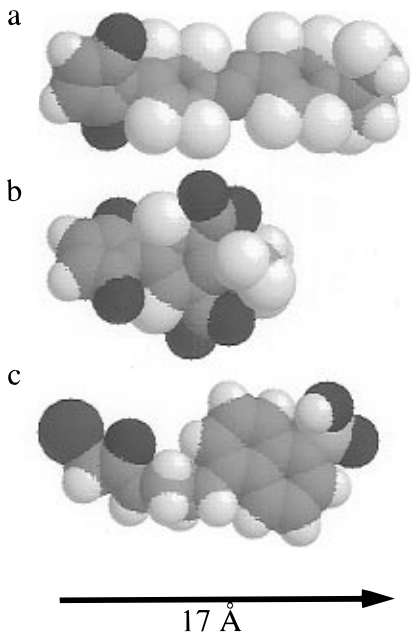

FIGURE 6: Representation of the structures of the probes used in this study. (a) DABMI; (b) DDPM; and (c) 1,5-IAEDANS. The left ends of the probes react with Cys-374. These structures have been obtained by energy minimization using Cerius[2] software and represent an extended configuration of these probes.

probably due to the difference in size and structure of the two acceptor probes as illustrated in Figure 6a,b.

Change in Fluorescence Due to the Binding of S-1. There is a small increase in the lifetime of 1,5-IAEDANS with no acceptor from 20.1 to 20.7 ns when either S1A1 or S1A2 is added to F-actin (Table 3). Also, when the steady-state data are corrected for the addition of S-1, the fluorescence intensity of the 1,5-IAEDANS F-actin solution increases by 14% with no shift of the emission peak (data not shown). This change in quantum yield of the probe results in a small increase of the R_0 value from 42.8 to 43.7 Å for the 1,5-IAEDANS−DABMI probe pair and from 29.0 to 29.6 Å for the 1,5-IAEDANS−DDPM pair.

Radial Coordinate of Cys-374 upon S-1 Binding. Similar FRET data were obtained for F-actin with both myosin S-1 isoforms as illustrated in Table 3. The lifetimes for the different AMF calculated for F-actin in the presence of S1A1 are not significantly different from those obtained in the presence of S1A2. Therefore, data from both isoforms were pooled (S-1). In the presence of S-1, 1,5-IAEDANS exhibited longer lifetimes (Table 3), reflecting smaller transfer efficiencies. This was also found with the steady-state measurements where the efficiency of transfer decreases by 23% with DABMI and by 9% with DDPM as acceptors (Table 4). The calculated radii for DABMI (AMF = 0.4) and DDPM (AMF = 0.42) are 24 and 17 Å, respectively. However, the increase in quantum yield of the donor probe may have been slightly underestimated in the steady-state measurements due to the increase of scattering of the solution when S-1 binds to F-actin. This would result in an underestimation of R_0 and consequently of their radii. In all of these experiments, the effect of light scattering was reduced by using a cuvette with a short light path (2 mm). Moreover, similar results were obtained using lifetime measurements which are not as much affected by light scattering. The change in the radial coordinates of the probes bound to Cys-374 is illustrated by the open circles in Figure 5, showing an increase from 13.5 to 16−23 Å. Addition of excess ATP results in a decrease in the lifetime of the donor to 14.3 ns which is close to but not equal to the value for F-actin without S-1 (Table 3). This difference can result from the dilution of the samples after addition of MgATP, therefore reducing the donor concentration. In the samples with high acceptor molar fraction, the donor concentration is far less than in the control samples, and close to the detection limit of our apparatus, resulting in a low signal to noise ratio. The effect of light scattering will then be more pronounced in the high AMF samples, resulting in an apparent decrease of the fluorescence lifetime. An increase of transfer efficiency was also observed for the steady-state fluorescence intensity measurements (Table 4). These data demonstrate that the changes in the radial coordinates of the probe bound to Cys-374 when S-1 binds are reversible.

DISCUSSION

Validation of the κ^2 Assumption in F-Actin. Censullo et al. (1992) employed a Dale−Eisinger analysis to obtain the limits on the average orientation factor κ^2 required to calculate molecular distances in F-actin using FRET measurements. In their analysis, they used dipole cone half-angles rather than depolarization factors, and the calculations assumed the restrictive condition of one electric dipole moment per probe. They showed that, for multiple acceptors in F-actin and without knowledge of the dipole orientations, $\kappa^2 = {}^2/_3$. Due to the multiplicity of acceptors in F-actin FRET experiments, less motion is required of the probes in order to apply $\kappa^2 = {}^2/_3$. Thus, in our results, it seems reasonable to assume this value.

Do Our FRET Data Agree with the Prediction from Models of F-Actin? In the Lorenz et al. refinement of the Holmes model of F-actin (Lorenz et al., 1993), the Sγ atom of Cys-374 is located at a radial coordinate of 27 Å. Given the size of the probe (Figure 6a), the radius obtained with the 1,5-IAEDANS−DABMI probe pair (17 Å) is compatible with the Sγ location in the Lorenz model. However, the smaller radius obtained with the smaller DDPM probe does not seem to support that model, even if we consider the worst case where the two probes 1,5-IAEDANS (Figure 6c) and DDPM (Figure 6b) are fully extended and oriented toward the center of the filament. The maximum radius obtained under these conditions would be ≈24 Å. Thus, Cys-374 may be located closer to the filament axis than proposed in the Lorenz model. However, we cannot rule out the possibility that changes in the hydrophobicity in the C-terminus, resulting from actin labeling, modify the position of the C-terminus and could explain the differences between the FRET results and the F-actin model.

Can the S-1-Induced Change in the Cys-374 Radial Coordinate Be Due to a Reposition of the Probe? It is unlikely that the change in radial coordinate of the probe results solely from a change in the probe position without any changes in the structure of the C-terminus of actin. Indeed, to accommodate a 4−5 Å change in radial coordinate, the two probes must reposition so that their dipole moments are located 4−5 Å closer to the periphery of the filament. This could explain our data for a large probe like DABMI but not for a small one (DDPM). We observed the same change in radius for both acceptor probes, and, therefore, most if not all of the change in the average position

(8−10 Å) must be attributed to the donor probe 1,5-IAEDANS. The fluorescence lifetime and intensity of F-actin labeled only with the donor probe increase by 4−14% when S-1 binds. Thus, the environment of the probe is not dramatically different in the presence or absence of S-1 This is consistent with a small change in position but not with a large reposition of the donor probe which would significantly alter its environment. Therefore, it is probable that the change of the average position of the dipole moment of the probe reflects a true change in the position of Cys-374. This agrees with the change in the position of the C-terminus upon S-1 binding proposed by Orlova and Egelman (1995). However, our data do not necessarily confirm the shift of electron density observed between subdomains 1 and 4.

The Same Changes Are Observed with either S1A1 or S1A2. The N-terminal 41 residues of myosin light chain 1 are absent in myosin light chain 3, and these residues have been shown to interact with residues 360, 362, 363, and 374 of the C-terminal region of actin (Trayer et al., 1987). Thus, we expected a change in the lifetime of a probe attached to the C-terminus when S1A1 or S1A2 binds to F-actin. Our data show that this is not the case since the efficiency of energy transfer is similar between the two isoforms. This finding suggests that the N-terminus of myosin light chain 1 does not directly interact with the C-terminus of actin as proposed by Xiao et al. (1996) and that its change in conformation must be allosteric.

Direct Contact of S-1 with the C-Terminus of Actin? It has been shown that pyrenyl-labeled Cys-374 interferes with S-1 binding (Blanchoin et al., 1996) and that when S-1 binds to pyrenyl-labeled F-actin it quenches its fluorescence intensity by 70% (Kouyama & Mihashi, 1981). We observed little change in 1,5-IAEDANS quantum efficiency when S-1 binds. These differences may be explained by the large size of the pyrenyl probe which might allow a direct interaction with S-1. However, we cannot rule out the possibility of a direct interaction of S-1 with other residues at the actin C-terminus. S-1 could interact with Phe-375 or with residues other than Cys-374 without interfering with the probes.

Comparison of FRET with Spin-Label Experiments. Spin-labels attached to Cys-374 apparently do not detect major conformational changes in this region upon S-1 binding (Ostap et al., 1992; Naber et al., 1994). This discrepancy with our results can be due to at least three inherent features of the EPR method: (1) a translation of a spin probe without a change in angle and Gaussian distribution would not be detected; (2) if the full width at half-maximum of the Gaussian distribution is large, e.g., 20° (Ostap et al., 1992), small changes in the mean angle would be difficult to detect; and (3) if the probe is oriented at or about 90° to the plane of the movement, no changes will be detected, whereas probes oriented parallel to that plane would detect a change (Roopnarine et al., 1993). Therefore, probes oriented at 32° (Ostap et al., 1992) and 36° (Naber et al., 1994) to the filament axis will detect proportionally smaller changes, assuming that the probe movement is close to a plane passing through the filament axis. Thus, our results are not necessarily incompatible with those obtained with spin-labels.

Conformational Changes of Subdomain 1 of Actin Extending to the C-Terminus. Cross-linking of Cys-374 to Lys-191 of the adjacent subunit along the short pitch helix is inhibited by S-1 binding (Knight & Offer, 1980) which indicates that S-1 perturbs the C-terminus of actin. A perturbation of the C-terminus involving movement of Cys-374 may be an allosteric effect, reflecting a much larger conformational change. Movements of subdomain 1 have been inferred from X-ray diffraction data when tropomyosin binds to F-actin (AL-Khayat et al., 1995). Thus, our observed changes may reflect a global change in actin subdomain 1 or in the so-called small domain of actin (comprising subdomains 1 and 2). This would be consistent with the changes in the radial coordinate of Gln-41 and the increase in distance between the nucleotide site and Tyr-69.

ACKNOWLEDGMENT

We are grateful to Louise Brown and Murat Kekic, who kindly provided some of the S-1 isoforms used in this study. We are also grateful to Nicole Bordes and the staff of Vislab for their help with the Cerius[2] software. We thank Brett Hambly and our colleagues in the Muscle Research Unit for helpful discussions.

REFERENCES

AL-Khayat, H. A., Yagi, N., & Squire, J. M. (1995) *J. Mol. Biol. 252*, 611−632.
Barden, J. A., & dos Remedios, C. G. (1984) *J. Biochem. 96*, 913−921.
Barden, J. A., & dos Remedios, C. G. (1987) *Eur. J. Biochem. 168*, 103−109.
Blanchoin, L., Didry, D., Carlier, M.-F., & Pantaloni, D. (1996) *J. Biol. Chem. 271*, 12380−12386.
Bradford, M. M. (1976) *Anal. Biochem. 72*, 248−254.
Censullo, R., Martin, J. C., & Cheung, H. C. (1992) *J. Fluoresc. 2*, 141−155.
Dalbey, R. E., Weiel, J., Perkins, W. J., & Yount, R. G. (1984) *J. Biochem. Biophys. Methods 9*, 251−266.
dos Remedios, C. G., & Cooke, R. (1984) *Biochim. Biophys. Acta 188*, 193−205.
dos Remedios, C. G., & Moens, P. D. J. (1995a) *Biochim. Biophys. Acta 1228*, 99−124.
dos Remedios, C. G., & Moens, P. D. J. (1995b) *J. Struct. Biol. 115*, 175−185.
dos Remedios, C. G., Miki, M., & Barden, J. A. (1987) *J. Muscle Res. Cell Motil. 8*, 97−117.
Holmes, K. C., Popp, D., Gebhard, W., & Kabsch, W. (1990) *Nature 347*, 44−49.
Hudson, E. N., & Weber, G. (1973) *Biochemistry 12*, 4145−4161.
Kabsch, W., Mannherz, H. G., Suck, D., Pai, E. F., & Holmes, K. C. (1990) *Nature 347*, 37−44.
Kasprzak, A. A., Takashi, R., & Morales, M. F. (1988) *Biochemistry 27*, 4512−4522.
Knight, P., & Offer, G. (1980) *Biochemistry 19*, 4682−4687.
Kouyama, T., & Mihashi, K. (1981) *Eur. J. Biochem. 114*, 33−38.
Lorenz, M., Popp, D., & Holmes, K. C. (1993) *J. Mol. Biol. 234*, 826−836.
Mannherz, H. G., Kabsch, W., & Leberman, J. (1977) *FEBS Lett. 73*, 141−143.
McLaughlin, P. J., Gooch, J. T., Mannherz, H. G., & Weeds, A. G. (1993) *Nature 364*, 685−692.
Mendelson, R. A., & Morris, E. (1994) *J. Mol. Biol. 240*, 138−154.
Miki, M., & Mihashi, K. (1978) *Biochim. Biophys. Acta 533*, 163−172.
Miki, M., & dos Remedios, C. G. (1990) *Biochem. Int. 22*, 125−132.
Miki, M., & Kouyama, T. (1994) *Biochemistry 33*, 10171−10177.
Miki, M., Hambly, B. D., & dos Remedios, C. G. (1986) *Biochim. Biophys. Acta 871*, 137−141.
Moens, P. D. J., Yee, D., & dos Remedios, C. G. (1994) *Biochemistry 33*, 13102−13108.
Naber, N., Lorenz, M., & Cooke, R. (1994) *J. Mol. Biol. 236*, 703−709.
O'Donoghue, S. I., Miki, M., & dos Remedios, C. G. (1991) *Arch. Biochem. Biophys. 293*, 110−116.

Orlova, A., & Egelman, E. H. (1995) *J. Mol. Biol. 245*, 582−597.
Ostap, M. E., Yanagida, T., & Thomas, D. D. (1992) *Biophys. J. 63*, 966−975.
Prochniewicz-Nakayama, E., & Yanagida, T. (1990) *J. Cell Biol. 216*, 761−772.
Rayment, I., Rypniewski, W. R., Schmidt-Base, K., Smith, R., Tomchick, D. R., Benning, M. M., Winkelmann, D. A., Wesenberg, G., & Holden, H. M. (1993) *Science 261*, 50−58.
Roopnarine, O., Hideg, K., & Thomas, D. D. (1993) *Biophys. J. 64*, 1896−1907.
Schutt, C. E., Myslik, J. C., Rozycki, M. D., Goonesekere, N., & Lindberg, U. (1993) *Nature 365*, 810−816.
Spudich, J. A., & Watt, S. (1971) *J. Biol. Chem. 246*, 4866−4871.
Taylor, D. L., Reidler, J., Spudich, J. A., & Stryer, L. (1981) *J. Cell Biol. 89*, 362−367.
Tirion, M. M., Benavraham, D., Lorenz, M., & Holmes, K. C. (1995) *Biophys. J. 68*, 5−12.
Tonomura, Y., Appel, P., & Morales, M. F. (1966) *Biochemistry 5*, 515−521.
Trayer, I. P., Trayer, H. R., & Levine, B. A. (1987) *Eur. J. Biochem. 164*, 259−266.
Van Der Meer, W. B., Coker, G., III, & Chen, S. S.-Y. (1994) *Resonance Energy Transfer, Theory and Data*, VCH Publishers Inc., New York.
Weeds, A. G., & Taylor, R. S. (1975) *Nature 257*, 54−56.
Xiao, M., Tartakowski, A., Andreev, O. A., & Borejdo, J. (1996) *Biochemistry 35*, 523−530.
Yanagida, T., & Oosawa, F. (1978) *J. Mol. Biol. 126*, 507−524.

BI962588L